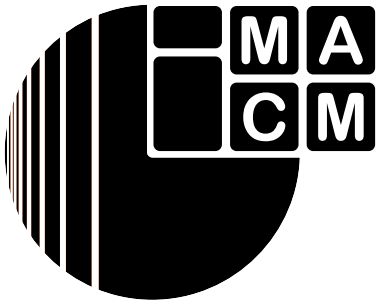

Bergische Universität Wuppertal

Fachbereich Mathematik und Naturwissenschaften

Institute of Mathematical Modelling, Analysis and Computational Mathematics (IMACM)

Preprint BUW-IMACM 12/33

Christof Kaufmann, Michael Günther, Daniel Klagges, Michael Knorrenschild, Matthias Richwin, Sebastian Schöps, Jan ter Maten

Efficient frequency-transient co-simulation of coupled heat-electromagnetic problems

December 2012

www-num.math.uni-wuppertal.de

Efficient frequency-transient co-simulation of coupled heat-electromagnetic problems

Christof Kaufmann[*] [†] Michael Günther[*]

Daniel Klagges[‡] Michael Knorrenschild[§]

Matthias Richwin[†] Sebastian Schöps[¶] Jan ter Maten[*] [‖]

16th December 2012

Background: With the recent advent of inductive charging systems all major automotive manufacturers develop concepts to wirelessly charge electric vehicles. Efficient designs require virtual prototyping that accounts for electromagnetic and thermal fields. The coupled simulations can be computationally very costly. This is because of the high frequencies in the electromagnetic part. This paper derives a mixed frequency-transient model as approximation to the original problem. We propose a co-simulation such that the electromagnetic part is simulated in the frequency domain while the thermal part resists in time domain.

Results: The iteration scheme for the frequency-transient model is convergent for low frequency and high frequency excitation. For sufficient high frequencies the iteration exhibits a quadratic convergence rate.

[*] Email: {kaufmann,guenther,termaten}@math.uni-wuppertal.de, Lehrstuhl für Angewandte Mathematik / Numerische Analysis, Bergische Universität Wuppertal, D-42119 Wuppertal, Germany

[†] Corresponding author

[‡] Email: {d.klagges,m.richwin@kostal.com}@kostal.com, Technology Development and Qualification – Simulation, Leopold Kostal GmbH & Co. KG, D-58513 Lüdenscheid, Germany

[§] Email: michael.knorrenschild@hs-bochum.de, Fachbereich Elektrotechnik und Informatik, Hochschule Bochum, D-44801 Bochum, Germany

[¶] Email: schoeps@gsc.tu-darmstadt.de, Graduate School of Computational Engineering, Technische Universität Darmstadt, D-64293 Darmstadt, Germany

[‖] Email: e.j.w.ter.maten@tue.nl, Dept. Mathematics & Computer Science, TU Eindhoven, PostBox 513, NL-5600 MB Eindhoven, The Netherlands

Conclusions: The frequency-transient model is very efficient for coupled heat-electromagnetic simulations since typically the time scales differ by several orders of magnitude. For medium frequencies large time steps can be chosen. The analysis shows, that for high frequencies the convergence rate improves further.

Keywords Inductive charging, Coupled simulation, Co-simulation, Electromagnetic, Heat, Modelling, Dynamic iteration

Mathematics Subject Classification 35K05, 35Q61, 65Z05, 78A25, 78M12, 80M25

1 Introduction

With the recent advent of inductive power charging systems and wireless power transmission in consumer and mobile phone technology, [1], all major automotive manufacturers develop concepts to wirelessly charge electric vehicles, both plug-in and pure electric vehicles (EV). For example the prototype from the Leopold Kostal GmbH & Co. KG of such an inductive charging station is shown in Fig. 1. The necessity to charge EVs with their current battery technology after every prolonged use – at least every night – is seen as one of the major drawbacks in the usability of EVs. A system to automate the charging process would reduce the burden on the driver; it could increase the acceptance of EVs, and, in the case of plug-in hybrid EVs, it could help to further reduce the CO_2 footprint since the battery of the plug-in hybrid could always be considered fully charged. This is important for the calculation of the fleet CO_2 emission.

A future inductive charging system does not necessarily exhibit a lower efficiency than a comparable conductive charging system, since there are only a few additional components; in a simplified view, the inductive charging system could be considered as a conductive charging system that has been cut in half in the middle of the transformer. For example the prototype from the Leopold Kostal GmbH & Co. KG of such an inductive charging station is shown in Fig. 1. There are, however, certain aspects that require attention and detailed design and optimization. These include positioning tolerances of the stationary ("primary") and car-mounted ("secondary") coils, magnetic stray fields, and thermal aspects.

The efficiency of both conductive and inductive charging systems is aimed well above 90 %, measured from the primary AC connection to the drive train battery. But even with this high efficiency, at 3.5 kW of first generation systems charging power there is a non-negligible amount of heat to be dissipated. Later generations with even higher power will further increase the heat load on the components. This heat load is the result of several different processes, namely resistance losses due to DC resistance and proximity effects, ferrite core losses and switching losses in the active semiconductor switching components. All effects appear at the same frequency as the magnetic field, which is of the order of 10 – 100 kHz. The resulting temperature however changes on much slower timescales, in the order of minutes, determined by

(a) Charge Station (b) Charging of a electric vehicle

Figure 1: Prototype of an inductive charging station, that charges the vehicle through its number plate (Images from Leopold Kostal GmbH & Co. KG).

the heat capacity and the (relatively large) mass of the involved components. This electromagnetic-thermal problem is fully coupled, as many of the material parameters show a significant thermal dependence. Typical ferrite core losses, for instance, are minimal at temperatures around 90°C and increase below and above this temperature. This drives the equilibrium temperature of the ferrite material always close to this temperature, if the dissipated power is small enough, or makes the system thermally unstable, if the heat power is too high.
Engineering samples of such systems are expensive, heavy, possibly dangerous to operate, and take a lot of time to build and optimize. Virtual prototyping using efficient simulation methods accelerates this process. There are different methodologies and models available, [2].
In Section 2, we propose a particular *frequency-transient model* for electromagnetic-thermal problems. The electromagnetic (EM) field is considered at high frequencies, where the time scale of the heat conduction is significantly lower than the time scale of the EM field. This can be exploited in the modeling. We propose a co-simulation scheme, similar to dynamic iteration [3], and analyze its convergence properties in Section 3. The analysis exhibits interesting results, especially for high frequencies. Possibilities to generalize this model are also discussed. Section 4 validates the results by a numerical simulation of a simplified model of the inductive charging system shown in Fig. 1.
In contrast to [2], where the different ways of co-simulation are discussed, we focus here on modeling and analysis of the *frequency-transient model*.

2 Modeling

In this section, we derive a model, which describes the electromagnetic field coupled to the temperature in the materials. For that, in Sec. 2.1 Maxwell's equations are introduced with temperature dependent material parameters. The conduction of the

heat is described in Sec. 2.2 by the heat equation together with an electromagnetic power term as source to describe the joule losses of the EM field. Finally, in Sec. 2.3 assumptions and approximations lead to the *frequency-transient model* [4].

2.1 Maxwell's Equations

Maxwell's equations read

$$\nabla \cdot \mathbf{D} = \rho \tag{1}$$

$$\nabla \cdot \mathbf{B} = 0 \tag{2}$$

$$\nabla \times \mathbf{E} = -\frac{\partial \mathbf{B}}{\partial t} \tag{3}$$

$$\nabla \times \mathbf{H} = \frac{\partial \mathbf{D}}{\partial t} + \mathbf{J} \tag{4}$$

where $\mathbf{E}$ and $\mathbf{H}$ are the electric and magnetic field strength, $\mathbf{D}$ and $\mathbf{B}$ are the electric and magnetic flux densities, ρ and $\mathbf{J}$ are the electric charge and current densities. These laws are supported by the constitutive relations

$$\mathbf{D} = \varepsilon\,\mathbf{E}, \qquad \mathbf{B} = \mu\,\mathbf{H} \quad \text{and} \quad \mathbf{J} = \sigma(T)\,\mathbf{E} + \mathbf{J}_{\text{src}},$$

where $\mathbf{J}_{\text{src}}$ describes an external source current density, the permittivity ε and permeability μ parameters depend only on space while the conductivity σ may also depend on the temperature T. In this way the EM field solution is a function of the temperature distribution (parameter coupling). Now to reduce the unknown in Maxwell's equations, we introduce the magnetic vector potential $\mathbf{A}$ and the electric scalar potential φ as

$$\mathbf{E} = -\nabla\varphi - \frac{\partial \mathbf{A}}{\partial t} \qquad \text{with} \qquad \mathbf{B} = \nabla \times \mathbf{A}.$$

By using these potentials, (2) and (3) are fulfilled automatically. From (4) we get

$$\nabla \times (\mu^{-1}\,\nabla \times \mathbf{A}) + \varepsilon\,\frac{\partial^2 \mathbf{A}}{\partial t^2} + \sigma(T)\,\frac{\partial \mathbf{A}}{\partial t} + \varepsilon\,\nabla\,\frac{\partial \varphi}{\partial t} + \sigma(T)\,\nabla\varphi = \mathbf{J}_{\text{src}}.$$

With Buchholz gauge transformation ($\nabla\varphi = 0$) this reduces to

$$\nabla \times (\mu^{-1}\,\nabla \times \mathbf{A}) + \varepsilon\,\frac{\partial^2 \mathbf{A}}{\partial t^2} + \sigma(T)\,\frac{\partial \mathbf{A}}{\partial t} = \mathbf{J}_{\text{src}}. \tag{5}$$

2.2 Heat Equation

The classical heat equation describes conduction of heat in materials:

$$\rho\,c\,\frac{\partial T}{\partial t} = \nabla \cdot (k \nabla T) + Q \tag{6}$$

with heat conductivity k, density ρ and specific heat capacity c, all constant in time. The term Q represents the joule losses of the EM field. Hence we use a source coupling

to connect the heat equation with the EM curl-curl equation (5). For simplicity we consider only eddy-current and joule losses and thus obtain

$$Q(\mathbf{A},T) = \mathbf{J}\cdot\mathbf{E} = \sigma(T)\,\mathbf{E}\cdot\mathbf{E} + \mathbf{J}_{\mathrm{src}}\cdot\mathbf{E} = \sigma(T)\,\frac{\partial\mathbf{A}}{\partial t}\cdot\frac{\partial\mathbf{A}}{\partial t} - \mathbf{J}_{\mathrm{src}}\cdot\frac{\partial\mathbf{A}}{\partial t}. \tag{7}$$

This power term is simplified in the next section.

2.3 Frequency-Transient Model

Now we aim at a model which allows an efficient simulation. The model consisting of (5) and (6) with (7) is defined in the time domain. A multirate co-simulation scheme could simulate both equations with different time steps. However, for a fast varying source current density the main part of the computational costs is caused by the simulation of (5). A discussion of single-rate and multirate schemes can be found in [2]. We will reduce these costs further by refining the model.
Since the temperature is only slowly varying in comparison to the EM field in (5) the temperature T, where σ is evaluated at, can be averaged by

$$\tilde{T}_i = \frac{1}{\tau_{i+1}-\tau_i}\int_{\tau_i}^{\tau_{i+1}} T(t)\,dt.$$

Thus we use $\sigma(T(t)) \approx \sigma(\tilde{T}_i)$ for $t \in [\tau_i, \tau_{i+1}]$ and then (5) can be approximated by

$$\nabla\times(\mu^{-1}\,\nabla\times\mathbf{A}) + \varepsilon\,\frac{\partial^2\mathbf{A}}{\partial t^2} + \sigma(\tilde{T}_i)\,\frac{\partial\mathbf{A}}{\partial t} = \mathbf{J}_{\mathrm{src}}. \tag{8}$$

However, this is still in time domain. To allow a solution in frequency domain, we assume a time harmonic source current density

$$\mathbf{J}_{\mathrm{src}} = \frac{1}{2}\,\hat{\mathbf{J}}_{\mathrm{src}}\,e^{j\,\omega\,t} + \frac{1}{2}\,\overline{\hat{\mathbf{J}}_{\mathrm{src}}}\,e^{-j\,\omega\,t}, \tag{9}$$

where $\hat{\mathbf{J}}_{\mathrm{src}}$ is a complex phasor. It follows for μ and ε independent of $\mathbf{A}$ that

$$\mathbf{A}(t) = \frac{1}{2}\,\left(\hat{\mathbf{A}}_c(\tilde{T}_i)\,e^{j\,\omega\,t} + \overline{\hat{\mathbf{A}}_c(\tilde{T}_i)}e^{-j\,\omega\,t}\right), \tag{10}$$

where the complex phasor $\hat{\mathbf{A}}_c$ is the solution for $\hat{\mathbf{J}}_{\mathrm{src}}$. This means the amplitude is constant within the time interval $[\tau_i, \tau_{i+1}]$.
Let us look at (7) again, but now with the approximation $\sigma(T(t)) \approx \sigma(\tilde{T}_i)$. The dot product is the usual real inner product.

$$\begin{aligned} Q(\mathbf{A},T) =& \sigma(\tilde{T}_i)\,\frac{\partial\mathbf{A}}{\partial t}\cdot\frac{\partial\mathbf{A}}{\partial t} - \mathbf{J}_{\mathrm{src}}\cdot\frac{\partial\mathbf{A}}{\partial t} \\ =& -\sigma(\tilde{T}_i)\,\frac{\omega^2}{4}\left(\hat{\mathbf{A}}_c\cdot\hat{\mathbf{A}}_c\,e^{j\,2\,\omega\,t} - 2\,\hat{\mathbf{A}}_c\cdot\overline{\hat{\mathbf{A}}_c} + \overline{\hat{\mathbf{A}}_c}\cdot\overline{\hat{\mathbf{A}}_c}\,e^{-j\,2\,\omega\,t}\right) \\ & - j\,\frac{\omega}{4}\left(\hat{\mathbf{J}}_{\mathrm{src}}\cdot\hat{\mathbf{A}}_c\,e^{j\,2\,\omega\,t} - \hat{\mathbf{J}}_{\mathrm{src}}\cdot\overline{\hat{\mathbf{A}}_c} + \overline{\hat{\mathbf{J}}_{\mathrm{src}}}\cdot\hat{\mathbf{A}}_c - \overline{\hat{\mathbf{J}}_{\mathrm{src}}}\cdot\overline{\hat{\mathbf{A}}_c}\,e^{-j\,2\,\omega\,t}\right), \end{aligned}$$

where $\hat{\mathbf{A}}_c = \hat{\mathbf{A}}_c(\tilde{T}_i)$. Now we are interested in the mean power loss in the time interval $[\tau_i, \tau_{i+1}]$:

$$\tilde{Q}_i = \frac{1}{\tau_{i+1} - \tau_i} \int_{\tau_i}^{\tau_{i+1}} Q\left(\mathbf{A}(t), T(t)\right)\, dt. \tag{11}$$

and thus all parts with $e^{\pm j\, 2\, \omega\, t}$ vanish (for interval length being a multiple of the half period length, i. e. $(\tau_{i+1} - \tau_i) = c\, \frac{\pi}{\omega}$, where $c \in \mathbb{N}$). Then we are left with

$$\tilde{Q}_i(\tilde{T}_i) = \sigma(\tilde{T}_i)\, \frac{\omega^2}{2} \left\| \hat{\mathbf{A}}_c(\tilde{T}_i) \right\|_c^2 + \frac{\omega}{2}\, \mathrm{Im}\left(\hat{\mathbf{J}}_{\mathrm{src}} \cdot \overline{\hat{\mathbf{A}}_c(\tilde{T}_i)} \right). \tag{12}$$

Now the simplified curl-curl equation (8) can be considered in frequency domain (with vector potential $\hat{\mathbf{A}}_c = \hat{\mathbf{A}}_c(\tilde{T}_i)$) along with the simplified heat equation (14) left in time domain:

$$(j\, \omega\, \sigma(\tilde{T}_i) - \omega^2\, \varepsilon)\hat{\mathbf{A}}_c + \nabla \times (\mu^{-1}\, \nabla \times \hat{\mathbf{A}}_c) = \hat{\mathbf{J}}_{\mathrm{src}} \tag{13}$$

$$\rho\, c\, \frac{\partial T}{\partial t} = \nabla \cdot (k \nabla T) + \tilde{Q}_i(\tilde{T}_i), \tag{14}$$

The curl-curl equation is formulated with constant material parameters in frequency domain. Thus, only a linear, complex system has to be solved once for each time window, instead for each time step of the curl-curl equation in time domain. That is why this approach is computationally highly efficient.
For the low frequency range, where inductive effects dominate, usually the displacement current $\partial \mathbf{D}/\partial t \mathrel{\hat{=}} \omega^2 \varepsilon \hat{\mathbf{A}}$ can be disregarded. This is called magnetoquasistatic formulation. For details on these formulations we refer to [5]. Here we aim to encompass all frequency ranges. Therefore our model is based on the full Maxwell formulation (1)–(4).

3 Algorithm

We will now discuss the algorithm to simulate heat-EM problems with the frequency-transient model. After discretization, the model is solved in a Gauss-Seidel scheme, which can be interpreted as co-simulation. It is comparable with a dynamic iteration for time integration. Section 3.1 will briefly discuss the co-simulation scheme. In Sec. 3.2 the convergence analysis for the iteration is proved.

3.1 Method

The co-simulation scheme uses (13) and (14) in a discretized form. For simplicity we assume Finite Integration Technique (FIT) [6–8] for spatial discretization and then for time discretization the implicit Euler method. The equations are of dimension n. As alternative to FIT discretization, one could use the Finite Element or Boundary Element Methods [9, 10]. In FIT-notation the curl-curl equation (13) becomes

$$\left(j\, \omega\, \mathbf{M}_\sigma^l - \omega^2\, \mathbf{M}_\varepsilon + \mathbf{C}^\top \mathbf{M}_\nu \mathbf{C}\right) \widehat{\mathbf{a}}^{l+1} = \widehat{\widehat{\mathbf{j}}}_{\mathrm{s}}, \tag{15}$$

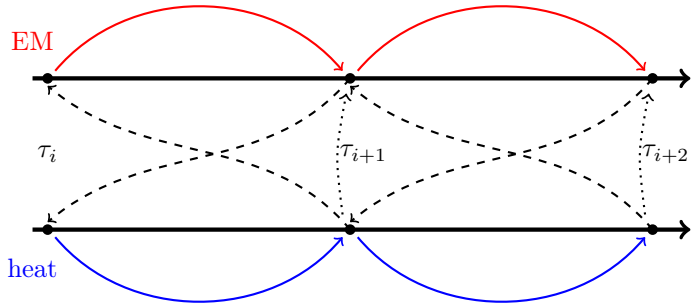

Figure 2: Frequency-transient co-simulation approach.

with diagonal positive semi-definite matrix for electric conductivity $\mathbf{M}_\sigma$, diagonal positive definite matrices for permittivity and reluctivity $\mathbf{M}_\epsilon$, $\mathbf{M}_\nu$, discrete curl operators $\mathbf{C}$, $\mathbf{C}^\top$ and the discretized (edge-integrated) magnetic vector potential $\widehat{\mathbf{a}}$. Note, that $\mathbf{M}_\sigma^l := \mathbf{M}_\sigma(\mathbf{T}^l)$, where $\mathbf{T}$ denotes the discretized temperature. For the heat equation, (14) gives

$$\left(\mathbf{M}_{\rho c} + h_i \tilde{\mathbf{S}} \mathbf{M}_k \tilde{\mathbf{S}}^\top\right) \mathbf{T}^{l+1} = \mathbf{M}_{\rho c} \mathbf{T}_i + h_i \frac{\omega}{2} \left[\omega \mathbf{M}_\sigma^{l+1} \mathbf{P} \widehat{\mathbf{a}}^{l+1} \circ \overline{\widehat{\mathbf{a}}^{l+1}} + \mathbf{P}\, \mathrm{Im}(\widehat{\mathbf{j}}_\mathrm{s} \circ \overline{\widehat{\mathbf{a}}^{l+1}})\right], \tag{16}$$

where $\circ$ denotes the Hadamard (element wise) product, with operator $\mathbf{P} \in \mathbb{R}^{n \times 3n}$ that transforms into point-wise norms, diagonal positive definite matrices for thermal conductivity and volumetric heat capacity $\mathbf{M}_k$, $\mathbf{M}_{\rho c}$, discrete divergence and gradient operators $\tilde{\mathbf{S}}$, $-\tilde{\mathbf{S}}^\top$ on the dual grid, respectively.

To simulate this model, (15) and (16) are solved successively. This can be repeated for one time step until convergence (see Alg. 1), similarly as done in Gauss-Seidel schemes. Here, we call it co-simulation. The scheme is also depicted in Fig. 2. However, since convergence cannot be guaranteed for such schemes in general, a proof is given in Sec. 3.2.

From Alg. 1 can be seen, that for each time step in the heat equation only one linear system has to be solved for the EM equation in frequency domain. This is the reason, why the model is very efficient.

3.2 Convergence Analysis

Theorem. *We assume given BC and IV and differentiability for $\mathbf{M}_\sigma$ w.r.t. temperature $\mathbf{T}$. Then the iteration is convergent for h_i small enough with*

$$\left\|\mathbf{T}^{l+1} - \mathbf{T}^*\right\| \leq C(\omega) h_i \left\|\mathbf{T}^l - \mathbf{T}^*\right\|,$$

where $C(\omega)$ is uniformly bounded on $\omega \in \mathbb{R}_+ \setminus [\omega_L, \omega_U]$, where the frequency gap $[\omega_L, \omega_U]$ depends on the discretization. Furthermore, for metals ($\mathbf{M}_\sigma' < 0$), we have $C(\omega) = \mathcal{O}\left(\frac{1}{\omega^2}\right)$ for large ω.

Algorithm 1 Co-Simulation with the frequency transient model, with discretized temperature $\mathbf{T}_i$, discretized magnetic vector potential $\widehat{\mathbf{a}}_i$ and time t_i.

1: Initialize model
2: $\mathbf{T}(t_0) \leftarrow \mathbf{T}_0$
3: $i \leftarrow 0$
4: **while** $t_i < t_{end}$ **do**
5: $\quad \mathbf{T}_{i+1}^0 \leftarrow \mathbf{T}_i$
6: $\quad l \leftarrow 0$
7: $\quad$ **while** $l < 2$ or not converged **do**
8: $\quad\quad$ Solve (15) for $\widehat{\mathbf{a}}_{i+1}^{l+1}$
9: $\quad\quad$ Solve (16) for $\mathbf{T}_{i+1}^{l+1}$
10: $\quad\quad l \leftarrow l + 1$
11: $\quad$ **end while**
12: $\quad \widehat{\mathbf{a}}_{i+1} \leftarrow \widehat{\mathbf{a}}_{i+1}^{l}$
13: $\quad \mathbf{T}_{i+1} \leftarrow \mathbf{T}_{i+1}^{l}$
14: $\quad i \leftarrow i + 1$
15: **end while**

Proof. Consider the inner loop of Alg. 1 (step 8 and 9). It consists of (15) and (16). We prove convergence for this inner loop. Beforehand we introduce some abbreviations:

$$\mathbf{X} := \omega^2 \, \mathbf{M}_\varepsilon - \mathbf{C}^\top \mathbf{M}_\nu \mathbf{C}, \qquad\qquad \mathbf{Z}^l := -\mathbf{X} + j\omega \, \mathbf{M}_\sigma^l.$$

Then (15) reads

$$\mathbf{Z}^l \widehat{\mathbf{a}}^{l+1} = \widehat{\overline{\mathbf{j}}}_s \tag{17}$$

$$\Leftrightarrow \quad \widehat{\mathbf{a}}^{l+1} = \left(\mathbf{Z}^l\right)^{-1} \widehat{\overline{\mathbf{j}}}_s \tag{18}$$

assuming that $(\mathbf{Z}^l)^{-1}$ exists. We define $\mathbf{N} := \tilde{\mathbf{S}} \mathbf{M}_k \tilde{\mathbf{S}}^\top$. Let us introduce an exact solution for $\mathbf{T}^l$ and $\widehat{\mathbf{a}}^l$ and denote it by $\mathbf{T}^*$ and $\widehat{\mathbf{a}}^*$, respectively. We use (16) with $\mathbf{T}^*$ and $\widehat{\mathbf{a}}^*$ subtract it from (16)

$$\begin{aligned}\left(\mathbf{M}_{\rho c} + h_i \mathbf{N}\right)\left(\mathbf{T}^{l+1} - \mathbf{T}^*\right) = h_i \frac{\omega^2}{2} \left(\mathbf{M}_\sigma^{l+1} \mathbf{P} \, \widehat{\mathbf{a}}^{l+1} \circ \overline{\widehat{\mathbf{a}}^{l+1}} - \mathbf{M}_\sigma^* \mathbf{P} \, \widehat{\mathbf{a}}^* \circ \overline{\widehat{\mathbf{a}}^*}\right) \\ + h_i \frac{\omega}{2} \mathbf{P} \operatorname{Im}\left(\widehat{\overline{\mathbf{j}}}_s \circ \overline{\left(\widehat{\mathbf{a}}^{l+1} - \widehat{\mathbf{a}}^*\right)}\right).\end{aligned} \tag{19}$$

Next, by adding and subtracting $h_i \frac{\omega^2}{2} \mathbf{M}_\sigma^* \, \mathbf{P} \, \widehat{\mathbf{a}}^{l+1} \circ \overline{\widehat{\mathbf{a}}^{l+1}}$, we have

$$\begin{aligned}\left(\mathbf{M}_{\rho c} + h_i \mathbf{N}\right)\left(\mathbf{T}^{l+1} - \mathbf{T}^*\right) = h_i \frac{\omega^2}{2} \left(\mathbf{M}_\sigma^{l+1} - \mathbf{M}_\sigma^*\right) \mathbf{P} \left(\widehat{\mathbf{a}}^{l+1} \circ \overline{\widehat{\mathbf{a}}^{l+1}}\right) \\ + h_i \frac{\omega^2}{2} \mathbf{M}_\sigma^* \, \mathbf{P} \left(\widehat{\mathbf{a}}^{l+1} \circ \overline{\widehat{\mathbf{a}}^{l+1}} - \widehat{\mathbf{a}}^* \circ \overline{\widehat{\mathbf{a}}^*}\right) + h_i \frac{\omega}{2} \mathbf{P} \operatorname{Im}\left(\widehat{\overline{\mathbf{j}}}_s \circ \overline{\left(\widehat{\mathbf{a}}^{l+1} - \widehat{\mathbf{a}}^*\right)}\right).\end{aligned} \tag{20}$$

Now, let us consider the term

$$\left(\mathbf{M}_\sigma^{l+1} - \mathbf{M}_\sigma^*\right) \mathbf{y}, \quad \text{where } \mathbf{y} := \mathbf{P} \, \widehat{\mathbf{a}}^{l+1} \circ \overline{\widehat{\mathbf{a}}^{l+1}}.$$

The conductivity matrix $\mathbf{M}_\sigma$ is a diagonal matrix for any iteration step. We assume, its k-th component σ_k depends only on the k-th component of the temperature, denoted by T_k. Therefore the k-th component of the term can be written as

$$\left(\sigma_k(T_k^{l+1}) - \sigma_k(T_k^*)\right) y_k,$$

where the index at σ_k should point to the fact, that there is a different conductivity function for each material. Now the mean value theorem can be applied component-wise and yields for the k-th component

$$\left(\sigma_k(T_k^{l+1}) - \sigma_k(T_k^*)\right) y_k = \sigma_k'(\zeta)\, y_k \left(T_k^{l+1} - T_k^*\right),$$

where $\zeta \in \left[T_k^{l+1}, T_k^*\right]$ and σ_k' is assumed to be negative. Hence, in matrix vector notation

$$\left(\mathbf{M}_\sigma^{l+1} - \mathbf{M}_\sigma^*\right)\mathbf{y} = \mathbf{M}_\sigma'(\zeta)\mathbf{Y}\left(\mathbf{T}^{l+1} - \mathbf{T}^*\right)$$

where the diagonal matrix $\mathbf{M}_\sigma'(\zeta)$ has only negative elements and $\mathbf{Y} := \operatorname{diag}(\mathbf{y})$. Then we can write (20) as

$$\begin{aligned}&\left(\mathbf{M}_{\rho c} + h_i\mathbf{N} - h_i\frac{\omega^2}{2}\mathbf{M}_\sigma'(\zeta)\operatorname{diag}\left(\mathbf{P}\,\widehat{\mathbf{a}}^{l+1}\circ\overline{\widehat{\mathbf{a}}^{l+1}}\right)\right)\left(\mathbf{T}^{l+1} - \mathbf{T}^*\right)\\ &= h_i\frac{\omega^2}{2}\mathbf{M}_\sigma^*\,\mathbf{P}\left(\widehat{\mathbf{a}}^{l+1}\circ\overline{\widehat{\mathbf{a}}^{l+1}} - \widehat{\mathbf{a}}^*\circ\overline{\widehat{\mathbf{a}}^*}\right) + h_i\frac{\omega}{2}\mathbf{P}\operatorname{Im}\left(\widehat{\widehat{\mathbf{j}}}_s\circ\overline{\left(\widehat{\mathbf{a}}^{l+1} - \widehat{\mathbf{a}}^*\right)}\right).\end{aligned} \tag{21}$$

Multiplying by the inverse of the matrix on the LHS and taking the norm yields

$$\begin{aligned}\left\|\mathbf{T}^{l+1} - \mathbf{T}^*\right\| \le{}& \left\|\left(\mathbf{M}_{\rho c} + h_i\mathbf{N} - h_i\frac{\omega^2}{2}\mathbf{M}_\sigma'(\zeta)\operatorname{diag}\left(\mathbf{P}\,\widehat{\mathbf{a}}^{l+1}\circ\overline{\widehat{\mathbf{a}}^{l+1}}\right)\right)^{-1}\right\|\\ &\cdot\left[h_i\frac{\omega^2}{2}\left\|\mathbf{M}_\sigma^*\,\mathbf{P}\left(\widehat{\mathbf{a}}^{l+1}\circ\overline{\widehat{\mathbf{a}}^{l+1}} - \widehat{\mathbf{a}}^*\circ\overline{\widehat{\mathbf{a}}^*}\right)\right\| + h_i\frac{\omega}{2}\left\|\mathbf{P}\operatorname{Im}\left(\widehat{\widehat{\mathbf{j}}}_s\circ\overline{\left(\widehat{\mathbf{a}}^{l+1} - \widehat{\mathbf{a}}^*\right)}\right)\right\|\right].\end{aligned} \tag{22}$$

Now, we need estimates for $\left\|\widehat{\mathbf{a}}^{l+1} - \widehat{\mathbf{a}}^*\right\|$ and for the quadratic term $\left\|\widehat{\mathbf{a}}^{l+1}\circ\overline{\widehat{\mathbf{a}}^{l+1}} - \widehat{\mathbf{a}}^*\circ\overline{\widehat{\mathbf{a}}^*}\right\|$. Additionally properties of the inverse have to be considered.
We start with the linear term by considering (17) with the exact solution and subtracting by (15)

$$\begin{aligned}&j\,\omega\,\mathbf{M}_\sigma^l\,\widehat{\mathbf{a}}^{l+1} - j\,\omega\,\mathbf{M}_\sigma^*\widehat{\mathbf{a}}^* - \mathbf{X}\left(\widehat{\mathbf{a}}^{l+1} - \widehat{\mathbf{a}}^*\right) = 0\\ \Leftrightarrow\quad &\mathbf{Z}^*\left(\widehat{\mathbf{a}}^{l+1} - \widehat{\mathbf{a}}^*\right) + j\,\omega\,\left(\mathbf{M}_\sigma^l - \mathbf{M}_\sigma^*\right)\widehat{\mathbf{a}}^{l+1} = 0\end{aligned}$$

$$\begin{aligned}\Rightarrow \left\|\widehat{\mathbf{a}}^{l+1} - \widehat{\mathbf{a}}^*\right\| &\le \omega\left\|\left(\mathbf{Z}^*\right)^{-1}\right\|\left\|\mathbf{M}_\sigma^l - \mathbf{M}_\sigma^*\right\|\left\|\widehat{\mathbf{a}}^{l+1}\right\|\\ &\le \omega\,\left\|\left(\mathbf{Z}^*\right)^{-1}\right\|\left|\sigma'_{\max}\right|\left\|\mathbf{T}^l - \mathbf{T}^*\right\|\left\|\left(\mathbf{Z}^l\right)^{-1}\right\|\left\|\widehat{\widehat{\mathbf{j}}}_s\right\|.\end{aligned}$$

For $\omega > \omega_U$ for some ω_U the matrix $\mathbf{X}$ is real, symmetric positive definite and $\mathbf{M}_\sigma$ is real, diagonal, positive semi-definite. Then

$$\mathbf{Z} = (-\mathbf{X} + j\omega\,\mathbf{M}_\sigma) = \mathbf{X}^{1/2}(-\mathbf{I} + j\,\omega\,\mathbf{X}^{-1/2}\mathbf{M}_\sigma\mathbf{X}^{-1/2})\mathbf{X}^{1/2}, \tag{23}$$

where $\mathbf{X}^{1/2} := \mathbf{U}\mathbf{\Sigma}^{1/2}\mathbf{U}^{-1}$ for an eigendecomposition $\mathbf{X} = \mathbf{U}\mathbf{\Sigma}\mathbf{U}^{-1}$.
Now let $\mathbf{A} := \mathbf{X}^{-1/2}\mathbf{M}_\sigma\mathbf{X}^{-1/2}$, which is real and symmetric positive definite. It follows that the eigenvalue decomposition is $\mathbf{A} = \mathbf{Q}^{-1}\mathbf{\Lambda}\mathbf{Q}$, with $\|\mathbf{Q}\| = 1$. Then

$$\begin{aligned}
\mathbf{Z}^{-1} &= \mathbf{X}^{-1/2}(-\mathbf{I} + j\,\omega\mathbf{A})^{-1}\mathbf{X}^{-1/2} \\
&= \mathbf{X}^{-1/2}(-\mathbf{Q}^{-1}\mathbf{Q} + j\,\omega\mathbf{Q}^{-1}\mathbf{\Lambda}\mathbf{Q})^{-1}\mathbf{X}^{-1/2} \\
&= \mathbf{X}^{-1/2}\mathbf{Q}^{-1}(-\mathbf{I} + j\,\omega\mathbf{\Lambda})^{-1}\mathbf{Q}\mathbf{X}^{-1/2} \\
\left\|\mathbf{Z}^{-1}\right\| &\leq \left\|\mathbf{X}^{-1/2}\right\| \left\|\mathbf{Q}^{-1}\right\| \left\|(-\mathbf{I} + j\,\omega\mathbf{\Lambda})^{-1}\right\| \left\|\mathbf{Q}\right\| \left\|\mathbf{X}^{-1/2}\right\| \\
&\leq \left\|\mathbf{X}^{-1/2}\right\| \cdot 1 \cdot \frac{1}{\sqrt{1+\omega^2\lambda_{\min}^2}} \cdot 1 \cdot \left\|\mathbf{X}^{-1/2}\right\| \leq \left\|\mathbf{X}^{-1}\right\|.
\end{aligned}$$

For $\omega < \omega_L$ for some ω_L, we define $\mathbf{Y} := -\mathbf{X}$, which is real, symmetric positive definite. Then analogue to (23)

$$\mathbf{Z} = (\mathbf{Y} + j\omega\,\mathbf{M}_\sigma) = \mathbf{Y}^{1/2}(\mathbf{I} + j\,\omega\,\mathbf{Y}^{-1/2}\mathbf{M}_\sigma\mathbf{Y}^{-1/2})\mathbf{Y}^{1/2},$$

where $\mathbf{Y}^{1/2} := \mathbf{U}\mathbf{\Sigma}^{1/2}\mathbf{U}^{-1}$ for an eigendecomposition $\mathbf{Y} = \mathbf{U}\mathbf{\Sigma}\mathbf{U}^{-1}$. However, this still yields $\left\|\mathbf{Z}^{-1}\right\| \leq \left\|\mathbf{Y}^{-1}\right\| = \left\|\mathbf{X}^{-1}\right\|$.
So in both cases

$$\begin{aligned}
\left\|\widehat{\mathbf{a}}^{l+1} - \widehat{\mathbf{a}}^*\right\| &\leq \omega \left\|\mathbf{Z}^{*-1}\right\| \left|\sigma'_{\max}\right| \left\|\mathbf{T}^l - \mathbf{T}^*\right\| \left\|\mathbf{X}^{-1}\right\| \left\|\widehat{\widehat{\mathbf{j}}}_s\right\| \\
&\leq c(\omega) \left\|\mathbf{T}^l - \mathbf{T}^*\right\|,
\end{aligned} \tag{24}$$

where $c(\omega) := \omega \left\|\left(j\,\omega\,\mathbf{M}_\sigma^* - \omega^2\,\mathbf{M}_\varepsilon + \mathbf{C}^\top\mathbf{M}_\nu\mathbf{C}\right)^{-1}\right\| \left|\sigma'_{\max}\right| \left\|\left(\omega^2\,\mathbf{M}_\varepsilon - \mathbf{C}^\top\mathbf{M}_\nu\mathbf{C}\right)^{-1}\right\| \left\|\widehat{\widehat{\mathbf{j}}}_s\right\|$.
We now consider the quadratic term in (22)

$$\begin{aligned}
\left\|\widehat{\mathbf{a}}^{l+1} \circ \overline{\widehat{\mathbf{a}}^{l+1}} - \widehat{\mathbf{a}}^* \circ \overline{\widehat{\mathbf{a}}^*}\right\| &= \left\|\left(\widehat{\mathbf{a}}^{l+1} - \widehat{\mathbf{a}}^* + \widehat{\mathbf{a}}^*\right) \circ \overline{\left(\widehat{\mathbf{a}}^{l+1} - \widehat{\mathbf{a}}^* + \widehat{\mathbf{a}}^*\right)} - \widehat{\mathbf{a}}^* \circ \overline{\widehat{\mathbf{a}}^*}\right\| \\
&\leq \left\|\left(\widehat{\mathbf{a}}^{l+1} - \widehat{\mathbf{a}}^*\right) \circ \overline{\left(\widehat{\mathbf{a}}^{l+1} - \widehat{\mathbf{a}}^*\right)}\right\| + 2\left\|\left(\widehat{\mathbf{a}}^{l+1} - \widehat{\mathbf{a}}^*\right) \circ \widehat{\mathbf{a}}^*\right\|.
\end{aligned}$$

Because $\|a \circ b\| \leq \|a\|\,\|b\|$, this can be written as

$$\begin{aligned}
\left\|\widehat{\mathbf{a}}^{l+1} \circ \overline{\widehat{\mathbf{a}}^{l+1}} - \widehat{\mathbf{a}}^* \circ \overline{\widehat{\mathbf{a}}^*}\right\| &\leq \left\|\widehat{\mathbf{a}}^{l+1} - \widehat{\mathbf{a}}^*\right\|^2 + 2\left\|\widehat{\mathbf{a}}^{l+1} - \widehat{\mathbf{a}}^*\right\| \left\|\widehat{\mathbf{a}}^*\right\| \\
&\leq c^2(\omega)\left\|\mathbf{T}^l - \mathbf{T}^*\right\|^2 + 2\,c(\omega)\left\|\widehat{\mathbf{a}}^*\right\| \left\|\mathbf{T}^l - \mathbf{T}^*\right\|,
\end{aligned} \tag{25}$$

where

$$\left\|\widehat{\mathbf{a}}^*\right\| = \left\|\left(\mathbf{Z}^*\right)^{-1}\widehat{\widehat{\mathbf{j}}}_s\right\| \leq \left\|\mathbf{X}^{-1}\right\| \left\|\widehat{\widehat{\mathbf{j}}}_s\right\|.$$

Finally we consider the inverse in (22). It holds

$$\left\|\left(\mathbf{M}_{\rho c} + h_i\mathbf{N} - h_i\frac{\omega^2}{2}\mathbf{M}'_\sigma(\zeta)\,\mathrm{diag}\left(\mathbf{P}\,\widehat{\mathbf{a}}^{l+1} \circ \overline{\widehat{\mathbf{a}}^{l+1}}\right)\right)^{-1}\right\| \leq \left\|\mathbf{M}_{\rho c}^{-1}\right\|, \tag{26}$$

since $\mathbf{M}_{\rho c}$, $\mathbf{N}$ and $-\mathbf{M}'_\sigma(\zeta)\,\mathrm{diag}\left(\mathbf{P}\,\widehat{\mathbf{a}}^{l+1} \circ \overline{\widehat{\mathbf{a}}^{l+1}}\right)$ are all positive definite.

Using the estimates (24), (25) and (26) in (22) gives

$$\left\|\mathbf{T}^{l+1}-\mathbf{T}^{*}\right\| \leq h_i \frac{\omega}{2} c(\omega) \left\|\mathbf{P}\right\| \left\|\mathbf{M}_{\rho c}^{-1}\right\| \left\|\mathbf{T}^{l}-\mathbf{T}^{*}\right\| \Big(\omega\, c(\omega) \left\|\mathbf{M}_{\sigma}^{*}\right\| \left\|\mathbf{T}^{l}-\mathbf{T}^{*}\right\| + 2\,\omega \left\|\mathbf{X}^{-1}\right\| \left\|\widehat{\widehat{\mathbf{j}}}_{s}\right\| \left\|\mathbf{M}_{\sigma}^{*}\right\| + \left\|\widehat{\widehat{\mathbf{j}}}_{s}\right\| \Big).$$

Now consider the asymptotic behavior of this for large ω and small h_i. It holds

$$c(\omega) = \omega \left\|\sigma'_{\max}\right\| \left\| \left(j\,\omega\,\mathbf{M}_{\sigma}^{*} - \omega^2\,\mathbf{M}_{\varepsilon} + \mathbf{C}^{\top}\mathbf{M}_{\nu}\mathbf{C} \right)^{-1} \right\| \left\| \left(\omega^2\,\mathbf{M}_{\varepsilon} - \mathbf{C}^{\top}\mathbf{M}_{\nu}\mathbf{C} \right)^{-1} \right\| \left\|\widehat{\widehat{\mathbf{j}}}_{s}\right\| \sim \frac{1}{\omega^3}$$

and

$$\left\|\mathbf{X}^{-1}\right\| = \left\| \left(\omega^2\,\mathbf{M}_{\varepsilon} - \mathbf{C}^{\top}\mathbf{M}_{\nu}\mathbf{C} \right)^{-1} \right\| \sim \frac{1}{\omega^2}.$$

Then, for fixed h_i and ω large enough, it follows that

$$\left\|\mathbf{T}^{l+1}-\mathbf{T}^{*}\right\| \leq h_i\, C(\omega) \left\|\mathbf{T}^{1}-\mathbf{T}^{*}\right\|,$$

with $C(\omega) \sim \frac{1}{\omega^2}$.
Unfortunately this result does not hold for small ω, where the terms $\omega^2\mathbf{M}_{\varepsilon}$ in $c(\omega)$ and $\left\|\mathbf{X}^{-1}\right\|$ are relatively small and do not contribute significantly to $C(\omega)$. Therefore, in this case $C(\omega)$ behaves like ω^2. □

The frequency gap occurs because of excitation frequencies that match the modal frequencies of the discretized curl-curl equation (15) itself. Then the system matrix becomes singular and the system has no longer a unique solution. However, in practice the time-harmonic approach can be used over a wide range of possible excitation frequencies, [11, 12]. For the Coulomb gauge and for the Lorenz gauge similar results are found. Also in pure transient simulation [13], a wide range of excitation frequencies is covered in practice.

3.3 Generalization

The frequency-transient model can be generalized in different ways. To enhance versatility, one can use a multifrequency excitation of the EM-equation. An application would be steel hardening of gears [14], where two frequencies are necessary to obtain a homogeneous heating of the surface. Also to approximate periodic signals other than sinusoidal, multifrequency excitation can be used. This also allows for a Harmonic Balance approach, which enables usage of a nonlinear permeability μ.

3.3.1 Time dependent phasor

The model can be improved by weakening the assumptions made. In [4] it is suggested to consider the complex phasor not as constant within one time window. This means (10) becomes

$$\mathbf{A}(t) = \frac{1}{2} \left(\hat{\mathbf{A}}_c(T)\, e^{j\,\omega\,t} + \overline{\hat{\mathbf{A}}_c(T)} e^{-j\,\omega\,t} \right) = Re\left(\hat{\mathbf{A}}_c(T)\, e^{j\,\omega\,t} \right). \tag{27}$$

Thus the derivatives are

$$\frac{\partial \mathbf{A}}{\partial t} = Re\left(\frac{\partial \hat{\mathbf{A}}_c}{\partial t} \cdot e^{j\,\omega\,t}\right) + Re\left(j\,\omega\,\hat{\mathbf{A}}_c \cdot e^{j\,\omega\,t}\right) \tag{28}$$

$$\frac{\partial^2 \mathbf{A}}{\partial t^2} = Re\left(\frac{\partial^2 \hat{\mathbf{A}}_c}{\partial t^2} \cdot e^{j\,\omega\,t}\right) + 2\,Re\left(j\,\omega\,\frac{\partial \hat{\mathbf{A}}_c}{\partial t} \cdot e^{j\,\omega\,t}\right) - Re\left(\omega^2\,\hat{\mathbf{A}}_c \cdot e^{j\,\omega\,t}\right), \tag{29}$$

where $\hat{\mathbf{A}}_c := \hat{\mathbf{A}}_c(T)$. Substituting (27)–(29) into (5) yields

$$\nabla \times (\mu^{-1}\,\nabla \times \hat{\mathbf{A}}_c) + \varepsilon\left(\frac{\partial^2 \hat{\mathbf{A}}_c}{\partial t^2} + 2\,j\,\omega\,\frac{\partial \hat{\mathbf{A}}_c}{\partial t} - \omega^2\,\hat{\mathbf{A}}_c\right) + \sigma(T)\left(\frac{\partial \hat{\mathbf{A}}_c}{\partial t} + j\,\omega\,\hat{\mathbf{A}}_c\right) = \hat{\mathbf{J}}_{\mathrm{src}},$$

which is now a second order PDE with partial derivatives with respect to time as well. Note that in [4] magnetoquasistatic formulation is used, so there the modification yields a first order system. However, since now both parts (EM and heat) have to be time integrated, the co-simulation of these can be called dynamic iteration [3].
Due to the modification (12) changes to

$$\tilde{Q}(T) = \frac{\omega^2}{2}\sigma(T)\left\|\hat{\mathbf{A}}_c\right\|_c^2 + \frac{\omega}{2}\left[2\,\sigma\,\mathrm{Im}\left(\frac{\partial \hat{\mathbf{A}}_c}{\partial t} \cdot \overline{\hat{\mathbf{A}}_c}\right) + \mathrm{Im}\left(\hat{\mathbf{J}}_{\mathrm{src}} \cdot \overline{\hat{\mathbf{A}}_c}\right)\right] + \frac{1}{2}\left[\left\|\frac{\partial \hat{\mathbf{A}}_c}{\partial t}\right\|_c^2 + \mathrm{Re}\left(\overline{\hat{\mathbf{J}}_{\mathrm{src}}} \cdot \frac{\partial \hat{\mathbf{A}}_c}{\partial t}\right)\right].$$

The convergence analysis can be extended accordingly.

3.3.2 MPDAE approach

The Multirate Partial Differential Algebraic Equations (MPDAE) approach in [15] offers another type of generalization. It yields a fully time-domain model that introduces two time scales according to a fast and a slow component in the solution. For circuit simulation this can be exploited to efficiently determine envelope simulation in case of amplitude modulation. The method however also works for frequency modulation problems. For the coupled electromagnetics-heat problem the slow time scale comes from the heat equation, the fast time scale comes from the periodic source in the electromagnetic problem.

4 Frequency-Transient Co-Simulation

The frequency-transient model is used in an inductive charging system for electric vehicles. The charging station is modeled in a 2d-axisymmetric way by a primary coil for the station and a secondary coil for the car. Both coils include some ferrite. Additionally there is a steel slice. For details of the set up we refer to [2]. The geometry and simulation results are shown in Fig. 3.

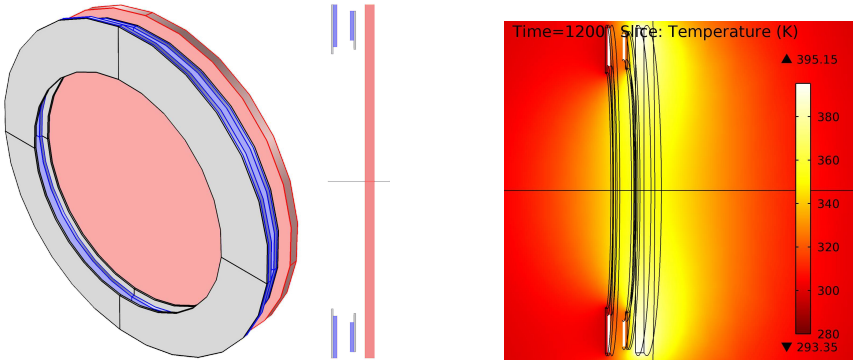

(a) 3d view and 2d cut view on geometry. From left to right: ferrite (gray), primary coil (blue), air, secondary coil (blue), ferrite (gray), air, steel slice (red). The left coil represents the charging station and the right coil the coil behind the number plate in the car.

(b) Temperature distribution after a simulation time of 20 min. The maximum temperature is 395.15 K.

Figure 3: Model for an inductive charging system for electric vehicles (Comsol).

The frequency-transient model proved to be very efficient. This is expected, since the main part of the computational effort – the time integration of the EM equation – is avoided. In fact the simulation time of 20 min could be reached by only 17 time steps. However, the Theorem in Sec. 3 requires to ensure convergence that the frequencies is sufficiently large. In this numerical example ω was chosen to be $2 \cdot \pi \cdot 10\,\mathrm{kHz}$ and it matched to the configuration (discretization, materials, current density, geometry). It is subject to further research to find the range for ω, s. t. the fixed-point iteration converges.

5 Conclusions

A frequency-transient model tailored for heat-electromagnetic problems was derived. The convergence analysis is drawn out in detail. It guarantees convergence for low and high frequencies. Higher frequencies benefit from a better convergence rate for the iteration. At low to moderate frequencies, simulation of the model is still efficient, due to the dimension of material parameters and spatial step size. This result also applies to approaches by Driesen and Hameyer [4] and similar implementations in Comsol [16]. Thus the approach fits perfectly for applications where inductive heating either appear as losses or is intended.

Competing interests

The authors declare that they have no competing interests.

Authors contributions

All authors contributed to this paper as a whole. However, special merits go to DK and MR for sharing their experiences from industry, which led to the numerical example and introduction; to SS and MG for the work on the model; to CK, JtM and MK for their contribution to the analysis. All authors read and approved the final manuscript.

Acknowledgements

This work is supported by the German BMBF in the context of the SOFA project (grant number 03MS648E). The sixth author is supported by the 'Excellence Initiative' of the German Federal and State Governments and the Graduate School of Computational Engineering at Technische Universität Darmstadt.

References

[1] Schneider D: **Wireless power at a distance is still far away [Electrons Unplugged]**. *IEEE Spectrum* 2010, **47**(5):34–39.

[2] Kaufmann C, Günther M, Klagges D, Richwin M, Schöps S, ter Maten J: **Coupled Heat-Electromagnetic Simulation of Inductive Charging Stations for Electric Vehicles** 2012. [Submitted for Proceedings ECMI 2012.].

[3] Bartel A, Brunk M, Günther M, Schöps S: **Dynamic Iteration for Coupled Problems of Electric Circuits and Distributed Devices**. *SIAM J Sci Comput* 2012. [Accepted].

[4] Driesen J, Hameyer K: **The simulation of magnetic problems with combined fast and slow dynamics using a transient time-harmonic method**. *Eur Phys J Appl Phys* 2001, **14**:165–169.

[5] Haus HA, Melcher JR: *Electromagnetic Fields and Energy*. Prentice Hall 1989, [http://web.mit.edu/6.013_book/www/].

[6] Clemens M, Gjonaj E, Pinder P, Weiland T: **Numerical simulation of coupled transient thermal and electromagnetic fields with the finite integration method**. *IEEE Trans. Magn.* 2001, **36**(4):1448–1452.

[7] Clemens M, Gjonaj E, Pinder P, Weiland T: **Self-consistent simulations of transient heating effects in electrical devices using the finite integration technique**. *IEEE Trans. Magn.* 2001, **37**(5):3375 –3379.

[8] Weiland T: **Time Domain Electromagnetic Field Computation with Finite Difference Methods** 1996, **9**(4):295–319.

[9] Bossavit A: *Computational Electromagnetism: Variational Formulations, Complementarity, Edge Elements*. San Diego: Academic Press 1998, [http://natrium.em.tut.fi/~bossavit/].

[10] Hiptmair R, Ostrowski J, Quast R: **Modelling and simulation of induction heating**. Tech. rep., SFB 382, University of Tübingen 2000.

[11] Hahne P, Weiland T: **3D eddy current computation in the frequency domain regarding the displacement current**. *IEEE Trans. Magn.* 1992, **28**(2):1801–1804.

[12] Clemens M, Weiland T: **Numerical algorithms for the FDiTD and FDFD simulation of slowly varying electromagnetic fields** 1999, **12**(1-2):3–22.

[13] Chen Q, Schoenmaker W, Chen G, Jiang L, Wong N: **A numerically efficient formulation for time-domain electromagnetic-semiconductor co-simulation for fast-transient systems**. *IEEE TCAD* 2012. [Accepted].

[14] Rudnev V: **Induction Hardening of Gears and Critical Components**. *Gear Technology* 2008, :58–63 (Sept/Oct) and 47–53 (Nov/Dec). [Part I and II.].

[15] Brachtendorf HG, Welsch G, Laur R, Bunse-Gerstner A: **Numerical steady state analysis of electronic circuits driven by multi-tone signals**. *Electrical Engineering (Archiv fur Elektrotechnik)* 1996, **79**:103–112. [10.1007/BF01232919].

[16] COMSOL Multiphysics: **Command Reference** 2007, [www.comsol.com].